Sensitivity analysis on turbulence models for the ABL in complex terrain

D. Cabezón
CENER, National Renewable Energy Centre, Wind Energy Department (Spain)
dcabezon@cener.com

J. Sanz
Von Karman Institute for Fluid Dynamics, Environmental and Applied Fluid Dynamics (Belgium)
sanz@vki.ac.be

J. Van Beeck
Von Karman Institute for Fluid Dynamics, Environmental and Applied Fluid Dynamics (Belgium)
vanbeeck@vki.ac.be

Abstract

One of the main features of the atmospheric surface layer is the fluctuating nature of wind and the rapid variation of some physical variables within the first meters in height. CFD codes have been adapted to simulate the behaviour of the atmospheric boundary layer (ABL) through different turbulence closure schemes associated with different turbulence models.

Some authors [6,10,15] have found good agreement with measurements of wind speed and turbulence intensity for some topologies in slightly complex terrain, mainly based on the Askervein hill test case. Nevertheless, very few studies have been made on more complex terrain [4,5] in order to check whether the turbulence models configurations used in non-complex terrain still holds.

After a grid dependency study, an optimized mesh is tested versus different turbulence closure schemes of two-equation k-ε turbulence models, using several sets of constants found in the literature. The standard K-ε model has been widely used because of its robustness and computing efficiency for a large variety of fluid applications. However, in the simulation of the ABL, overestimation of turbulence viscosity at steep areas with detached flows makes improved models, such as K-ε RNG or k-ε Realizable, more reliable. These models are also part of the study.

The performance of all the models is tested versus a measuring campaign at the hilltop of the Alaiz site, characterized by complex terrain and already presented in a previous conference [5]. The study will help to check in the near future whether there is a "universal" turbulence model configuration for complex terrain or whether the model is site dependent and requires calibration from onsite measurements.

Keywords: Alaiz Hill, kε turbulence models, CFD

1. Introduction

As larger wind farms are installed in complex terrain, it becomes harder to characterize the flow in order to assess wind speed and turbulence intensity at each wind turbine location. As a result, CFD solvers are being adapted to cope with the specific simulation of ABL flows. This topic has become essential when classifying wind turbine locations placed on complex terrain. The steep topography may produce unexpected low wind speeds and/or high turbulence intensities compromising the feasibility and lifetime of wind turbines.

The selection of the most appropriate closure scheme and the parameterization of the turbulent model are common issues to be considered. Two-equation closures have usually been employed such as the isotropic k-ε models for their robustness, computational efficiency and reasonable accuracy for a wide range of turbulent flows [8]. Since Launder and Spalding developed it in 1972, important advances have been made to improve its performance in the near wall region by developing new models like those based on Renormalization Group Techniques (RNG) (Yakhot & Orszag 1986, Choudhury 1993) and the so-called Realizable (Shih, Liou at al, 1995). These models are specially suited for rapidly strained flows at areas of strong curvature where the turbulent viscosity ratio tends to be overestimated by the standard model. Despite these new developments, different authors have attempted to modify the original standard model in order to resolve better the ABL by using different combinations of constants (Detering & Etling 1985, Duynkerke 1988, Richards & Hoxey 1993, Beljaars 1987, etc.).

The Askervein hill test case [13] was an extensively instrumented site which has allowed modellers to analyze the most influential parameters on the simulation of ABL flows in order to asess numerical codes. Several authors have reported accurate fits with experimental values upstream, with significant discrepancies near the hilltop and on the lee side where flow recirculation might be present.

Kim & Pattel [10] simulated the Askervein hill using Reynolds Averaged Navier Stokes (RANS) equations based on standard k-ε model (with default and modified constants) and RNG turbulence closure. The best predictions were obtained with the RNG model. Precise evolution of the fractional speed-up ratio over Askervein hill was found. The worst problems were found in the correct simulation of the turbulence kinetic energy, with important underestimation on the lee side of the hill, where the flow is likely to present intermittent separation. Similar results have been

recently reported by Undheim [15] also using the RNG model on the Askervein case. A strong influence on the accuracy of predictions was found for the vertical resolution and the height of the first grid cell.

Castro el. al. [6] arrived at similar conclusions regarding the importance of the vertical discretization. They used the standard k-ε model with the modified constants provided by Beljaars et al. [2]. The upstream overprediction on the turbulence kinetic energy was explained as an inability of the standard k-ε model to accommodate the effects of the streamline curvature, making the turbulent viscosity ratio increase where rapid distortion of the flow occurs.

This paper aims to review the different modelling strategies found in the literature using RANS turbulence models on non-complex terrain and test them on a significantly more complex site. Fluent 6.2, the commercial CFD solver, will be used, explaining the adopted modelling strategy. In particular, the adaptation of the wall functions to ABL flows will be discussed in detail. The turbulence models will be compared with each other and against field measurements at three mast positions.

2. Turbulence modelling of the ABL

Turbulent behaviour of a neutrally stratified ABL has been traditionally modelled making use of different turbulent closures which generalize the behaviour of the air as an incompressible fluid in steady state. The Navier Stokes equations of continuity (1) and momentum (2) in RANS form are:

$$\frac{\partial}{\partial x_i}(\rho u_i) = 0 \tag{1}$$

$$\frac{\partial}{\partial x_j}(\rho u_i u_j) = -\frac{\partial p}{\partial x_i} + \frac{\partial}{\partial x_j}\left[\mu\left(\frac{\partial u_i}{\partial x_j} + \frac{\partial u_j}{\partial x_i} - \frac{2}{3}\delta_{ij}\frac{\partial u_l}{\partial x_l}\right)\right] + \frac{\partial}{\partial x_j}\left(-\rho\overline{u_i' u_j'}\right) \tag{2}$$

where the so called Reynolds stresses $-\rho\overline{u_i' u_j'}$ are modelled by using the Boussinesq hypothesis which relates them to the mean velocity gradients through a parameter called turbulent viscosity μ_t.

$$-\rho\overline{u_i' u_j'} = \mu_t\left(\frac{\partial u_i}{\partial x_j} + \frac{\partial u_j}{\partial x_i}\right) - \frac{2}{3}\left(\rho k + \mu_t\frac{\partial u_i}{\partial x_i}\right)\delta_{ij} \tag{3}$$

Isotropic two-equation closure has proved to be accurate enough when integrating it into CFD offering acceptable errors and computing time. Hence k-ε models are widely used although they find problems in the near wall region where wind turbines are found. That is why many authors have proposed changes to the original model (Launder & Spalding 1972) by modifying the constants associated to the standard version and even altering the original equations giving as a result the RNG or the Realizable model.

Unsteady RANS models and other more sophisticated turbulence models like Reynolds Stress Model (RSM) or Large Eddy Simulation (LES) are also available but their computing cost makes them only applicable at academic level for the moment.

2.1 Standard kε

2.1.1 Default constants. Launder & Spalding (1972)

This is the simplest of the k-ε models in which the solution of two separate transport equations allows the turbulent velocity and length scales to be independently determined [8]. As it was mentioned before, robustness economy and reasonable accuracy for a wide range of turbulent flows explains its popularity in solving industrial flows, including the ones affecting the ABL. It is a semi-empirical model and the derivation of its equations relies on phenomenological considerations and empiricism.

The turbulent kinetic energy k and dissipation rate ε are obtained from the following transport equations:

$$\frac{\partial}{\partial t}(\rho k) + \frac{\partial}{\partial x_i}(\rho k u_i) = \frac{\partial}{\partial x_i}\left[\left(\mu + \frac{\mu_t}{\sigma_k}\right)\frac{\partial k}{\partial x_j}\right] + G_k - \rho\varepsilon \tag{4}$$

$$\frac{\partial}{\partial t}(\rho\varepsilon) + \frac{\partial}{\partial x_i}(\rho\varepsilon u_i) = \frac{\partial}{\partial x_j}\left[\left(\mu + \frac{\mu_t}{\sigma_\varepsilon}\right)\frac{\partial \varepsilon}{\partial x_j}\right] + C_{1\varepsilon}\frac{\varepsilon}{k}G_k - C_{2\varepsilon}\rho\frac{\varepsilon^2}{k} \tag{5}$$

where G_k represents the generation of turbulent kinetic energy due to the mean velocity gradients and the turbulent viscosity is computed as follows:

$$\mu_t = \rho C_\mu \frac{k^2}{\varepsilon} \tag{6}$$

The default constants $C_\mu, C_{1\varepsilon}, C_{2\varepsilon}, \sigma_k, \sigma_\varepsilon$ correspond to the combination initially proposed by Launder & Spalding:

$$\boxed{C_\mu = 0.09, C_{1\varepsilon} = 1.44, C_{2\varepsilon} = 1.92, \sigma_k = 1.0, \sigma_\varepsilon = 1.3} \tag{7}$$

These constants have been determined from experiments with air and water for fundamental turbulent shear flows and they have been found to work fairly well for a wide range of flows [8].

2.1.2 Modified constants. Richards & Hoxey (1993)

Richards and Hoxey [12] proposed a set of constants based on field measurements.

$$\boxed{C_\mu = 0.012, C_{1\varepsilon} = 1.2, C_{2\varepsilon} = 1.92, \sigma_k = 1.0, \sigma_\varepsilon = 3.22} \tag{8}$$

They also state that the set of constants (8) is compatible with the transport equations (4) and (5) providing the following condition is met.

$$\sigma_\varepsilon = \frac{\kappa^2}{(C_{2\varepsilon} - C_{1\varepsilon})\sqrt{C_\mu}} \tag{9}$$

where κ is the von Karman constant $\kappa \approx 0.4$.

2.1.3 Modified constants. Panofsky & Dutton (1984)

This set is based on the measurements made by Panofsky and Dutton [11] on flat terrain for the ratios of standard deviations of velocity components to friction velocity, namely:

$$\frac{\sigma_x}{u_*} = 2.39 \qquad \frac{\sigma_y}{u_*} = 1.92 \qquad \frac{\sigma_z}{u_*} = 1.25 \tag{10}$$

These values have been universally accepted as characteristic for the normal components of the variances of air within the ABL (IEC 61400-1). From (10), an equivalent C_μ of 0.033 is obtained [1,4,7]. Keeping the values of $C_{2\varepsilon}$ and σ_k, of the standard model on (4) σ_ε= 1.3 is obtained after applying condition (9).

$$\boxed{C_\mu = 0.033, C_{1\varepsilon} = 1.176, C_{2\varepsilon} = 1.92, \sigma_k = 1.0, \sigma_\varepsilon = 1.3} \tag{11}$$

2.1.4 Modified constants. Detering & Etling (1985), Duynkerke (1988)

Kim & Pattel propose another set of constants modified by Detering and Etling in 1985 and later by Duynkerke in 1988. This set allowed the simulation of a neutrally and stably-stratified ABL, including the Coriolis effect on turbulence, and correcting the over-estimation of the eddy viscosity in the upper atmosphere where the wind shear is weaker [10].

$$\boxed{C_\mu = 0.033, C_{1\varepsilon} = 1.46, C_{2\varepsilon} = 1.83, \sigma_k = 1.0, \sigma_\varepsilon = 2.38} \tag{12}$$

The behaviour of the flow induced by this modified set of constants showed separation bubbles over triangular ridges much wider than the separation zones offered by the other configurations. Keeping von Karman constant $\kappa \approx 0.4$, this set satisfies accurately the condition (9).

2.1.5 Modified constants. Beljaars (1987)

This set proposed by Castro et al. [6] follows the recommendations by Beljaars et. al. [2] and keeps essentially the same values of C_μ offered by Panofsky and the default ones for $C_{1\varepsilon}$, $C_{2\varepsilon}$ and σ_k proposed on the original model, resulting in a σ_ε of 1.85. The condition (9) is also satisfied by the proposed set with $\kappa \approx 0.4$.

$$\boxed{C_\mu = 0.033, C_{1\varepsilon} = 1.44, C_{2\varepsilon} = 1.92, \sigma_k = 1.0, \sigma_\varepsilon = 1.85} \tag{13}$$

2.2 RNG kε model

The RNG model (Yakhot & Orszag 1986, Choudhury 1993) was derived using a rigorous statistical technique called renormalization group theory. Its form is similar to the standard model *k-ε*, but includes additional terms in its ε equation that significantly improves the accuracy for rapidly strained flows [8].

Thus when the mean strain tensor S_{ij} increases in areas of strong curvature, RNG decreases the constant $C_{2\varepsilon}$, augmenting the turbulent dissipation rate and consequently decreasing the turbulent kinetic energy as well as the turbulent viscosity ratio, which is overestimated in the near wall region by the standard model.

$$\frac{\partial}{\partial t}(\rho\varepsilon) + \frac{\partial}{\partial x_i}(\rho\varepsilon u_i) = \frac{\partial}{\partial x_j}\left(\alpha_\varepsilon \mu_{eff} \frac{\partial \varepsilon}{\partial x_j}\right) + C_{1\varepsilon}\frac{\varepsilon}{k}G_k - C^*_{2\varepsilon}\rho\frac{\varepsilon^2}{k} \tag{14}$$

where α_ε is the inverse effective Prandtl number. At high-Reynolds-number limit:

$$\alpha_\varepsilon\left(=\frac{1}{\sigma_\varepsilon}\right) = \alpha_k \approx 1.393 \tag{15}$$

$$C^*_{2\varepsilon} = C_{2\varepsilon} + \frac{C_\mu \eta^3 (1 - \eta/\eta_0)}{1 + \beta\eta^3} \tag{16}$$

where: $\eta = \frac{Sk}{\varepsilon}, S = \sqrt{2S_{ij}S_{ij,}}\,\eta_0 = 4.38, \beta = 0.012$

For ABL at high Reynolds numbers, the turbulent viscosity ratio is calculated through the same equation specified in (6) as in the standard model. The values of constants are summarized as follows:

$$\boxed{C_\mu = 0.085, C_{1\varepsilon} = 1.42, C_{2\varepsilon} = 1.68, \sigma_k = 0.7179, \sigma_\varepsilon = 0.7179} \tag{17}$$

This model has also been extensively used during the last years by several authors for the simulation of the ABL with good results [10,15].

2.3 Realizable kε model

The Realizable *k-ε* model (Shih et. Al, 1995) differs from the standard model in two important ways:

- A new turbulent viscosity formulation involving a variable C_μ as a function of the mean strain rate (supposing the mean rotation rate Ω_{ij} is negligible) and the turbulence fields in terms of *k* and *ε*. This new value is computed from:

$$C_\mu = \frac{1}{A_0 + A_s \dfrac{kU^*}{\varepsilon}} \tag{18}$$

where, $A_0 = 4.04 \qquad U^* = \sqrt{S_{ij}S_{ij}} \qquad A_s = F(S_{ij})$

- A new transport equation for the dissipation rate *ε*, derived from an exact equation for the transport of the mean vorticity fluctuation. The *k* equation is the same as that in the standard *k-ε* model and the RNG *k-ε* model, except for the model constants [8]. In the same way, the constant associated to the generation of *ε* is affected by the mean strain tensor, making the upper value to be limited according to the equation:

$$\frac{\partial}{\partial x_j}(\rho\varepsilon u_j) = \frac{\partial}{\partial x_j}\left[\left(\mu + \frac{\mu_t}{\sigma_\varepsilon}\right)\frac{\partial \varepsilon}{\partial x_j}\right] + \rho C_{1\varepsilon} S\varepsilon - \rho C_{2\varepsilon}\frac{\varepsilon^2}{k + \sqrt{\nu\varepsilon}} \tag{19}$$

where, $C_{1\varepsilon} = \max\left[0.43, \frac{\eta}{\eta + 5}\right] \qquad \eta = S\frac{k}{\varepsilon} \qquad S = \sqrt{2S_{ij}S_{ij}}$

An immediate benefit of the realizable *k-ε* model is that it more accurately predicts the spreading rate of both planar and round jets [8]. It is also likely to provide superior performance for flows involving rotation, strong streamline curvature, boundary layers under adverse pressure gradients, separation and recirculation.

The default model constants are:

$$\boxed{C_{1\varepsilon} = 1.44, C_{2\varepsilon} = 1.9, \sigma_k = 1.0, \sigma_\varepsilon = 1.2} \tag{20}$$

3. Test site. Data for validation

Alaiz site in figure 1 is located South of Pamplona (Navarra, Spain), with a main orientation east-west and 4km long, normal to the prevailing north wind direction.

The hill is approximately 1050 meters a.s.l. and immersed in complex terrain with an average ruggedness index of [1]RIX=16% from Alaiz3 mast (figure 1) [5]. In the prevailing wind direction from the North the slope is steep enough to accelerate the flow in such a way that the profile at the hilltop keeps on accelerating at the surface layer. Total height drop upstream is 500 meters. Downstream (towards the South) parallel valleys with a north-south axis develop from the hilltop. Several kilometres towards the west, the hill continues with a strong slope at the south whereas on the east side a peak of 1280 meters a.s.l. is found separated from the main site by a big channel.

The roughness level is high in the areas surrounding the hill, which is completely covered by dense forests (z_0~0.1m). The surface upwind towards the north is slightly roughed, so that roughness was considered as low and equivalent to clear terrain (z_0~0.03m).

Three meteorological masts were used for assessment: Alaiz2 (20m/40m), Alaiz3 (30m/40m/55m) and Alaiz6 (20m/40m). The data cover a 1-year period (Nov96-Nov97) corresponding to the measuring campaign of a wind farm installed on the site from 2000. The sensors (helicoidal propeller and direction vane assembled on the same device) recorded, during the specified period, 10-min averages of wind speed, wind direction and standard deviation for both of them with a sampling rate of 3 seconds. The analysis showed on this paper only analyses the prevailing wind direction from the North, i.e. only northerly data is used for the assessment tests (20º sector).

4. Simulation features

The commercial CFD solver Fluent 6.2 was employed using the steady-state RANS approximation, considering air as an incompressible fluid. Coriolis force as well as heat transfer effects were not taken into account so that only neutral steady state atmosphere is considered.

4.1 Computational domain

The most important geographical features were considered by generating a digital terrain model of 9x9 km^2 from a digitized map with 25m resolution.

After a grid dependency study, an optimized structured mesh was created with variable horizontal and vertical resolution. The highest resolution is found at the assessment site resulting a computational domain of approximately 9x9x5 km^3 composed of 260x234x60=3.65 million cells. Vertical resolution was given by a height of 0.5m for the first cell next to the ground, increasing to approximately 400 meters at 5000m a.s.l. (Fig. 1).

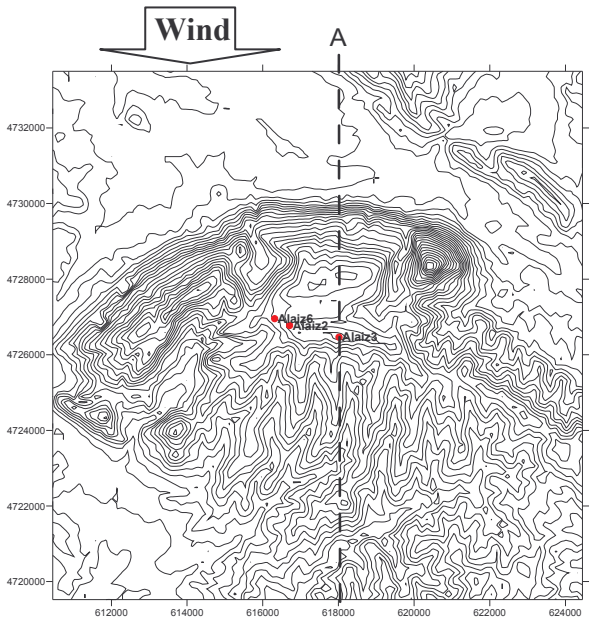

Figure 1: Alaiz hill site with 3 meterological masts and line A. Wind from the North. Coordinates in meters.

4.2 Boundary conditions

Richards and Hoxey [12] proposed appropriate boundary conditions, for computational wind engineering problems, which are compatible with the k-ε equations (4) and (5). Several assumptions were made in order to preserve this homogeneity, namely: 1) zero vertical velocity, 2) constant pressure, and 3) constant shear stress.

$$u = \frac{u_*}{\kappa}\ln\left(\frac{z}{z_0}\right) \qquad k = \frac{u_*^2}{\sqrt{C_\mu}} \qquad \varepsilon = \frac{u_*^3}{z+z_0} \tag{21}$$

The profiles (21) of wind speed, turbulent kinetic energy and turbulent dissipation rate, also constitute the inlet profiles of the present study. They are said to be fully developed profiles in equilibrium, i.e. free of streamwise gradients. It will be further discussed how these profiles adapt to the conditions defined at the wall through the use of wall functions.

The eastern and western boundaries as well as the top one were defined as symmetry (velocity parallel to boundary) whereas a pressure outlet boundary condition was used at the southern outflow boundary.

A wall boundary condition was assigned to the terrain surface. The boundary condition is applied through the standard wall functions implemented in Fluent 6.2.

4.3 Wall functions

The modeling of terrain roughness with CFD is carried out making use of the so-called wall functions. These functions model the region between the first node in the vertical direction and the wall. In this first layer, the flow experiences a transition from fully turbulent to laminar with zero velocity at the wall. The turbulent model, used above this layer, is essentially not valid in

[1] All RIX indexes at the present study are referred to North direction

the near-wall region as the regime is not fully turbulent. Besides, the use of wall functions avoids the discretization of this thin region, where the high velocity gradient would imply the use of a large number of cells.

The wall function definition also plays an important role in the inlet region. It is necessary that the wall function is compatible with the inlet velocity and turbulent production and dissipation profiles. Otherwise, the inlet profiles will be immediately modified to adapt to the new conditions imposed by the wall boundary. This compatibility problem has been recently addressed by Blocken et al. [3], on the simulation of neutrally stratified ABL over uniformly rough flat terrain also using the Fluent 6.2 solver.

CFD wall functions are normally based on the universal near-wall logarithmic velocity profile for turbulent flow over a smooth wall. The law of the wall is then modified using experimental data in order to include the important effect of the roughness. In the case of Fluent 6.2 the law-of-the-wall modified for roughness is based on experiments in sand-grain roughened pipes and channels [8]. The effect of the roughness is introduced by a shift ΔB of the intercept of the smooth law-of-the-wall.

$$u^+ = \frac{1}{\kappa}\ln\left(z^+\right) + B - \Delta B(k_s^+) \qquad (22)$$

$$u^+ = \frac{U}{u^*};\quad z^+ = \frac{u^* z}{\nu};\quad k_s^+ = \frac{u^* k_s}{\nu};\quad B \approx 5.2$$

In terms of the nondimensional height z^+, the log-law-of-the-wall is valid between z^+=30 and z^+=500-1000. Below, there is a laminar sublayer from the wall to z^+=5, where the linear profile $u+=z+$ holds, and a buffer region in between. The introduced roughness function ΔB depends on the dimensionless roughness height k_s^+ that, equivalent to a Reynolds number, defines the regime. In the case of ABL flows, the regime is always fully turbulent, i.e. k_s^+>90, and the roughness function takes the following form:

$$\Delta B = \frac{1}{\kappa}\ln\left(1 + C_s k_s^+\right) \qquad (23)$$

Therefore, the wall function modified for roughness is parameterized with the roughness height k_s and the roughness constant C_s ($0 \le C_s \le 1$). By continuity of velocity magnitude and gradient, of the wall function and ABL log-law at the first cell height z_p, Blocken et al. [3] derive a relationship between the ABL roughness length and Fluent roughness parameters C_s and K_s.

$$k_{s,ABL} = \frac{9.793 z_0}{C_s} \qquad (24)$$

No guidelines are given for the parameter C_s, so the default value is normally used C_s=0.5. Franke et al. [9] recommend $k_{s,ABL} \sim 30 z_0$. In both cases, the roughness height is more than one order of magnitude higher than the roughness length. For a roughness length of 3cm, typical value observed at the Alaiz site, the roughness height would be of the order of ks~0.6m. As stated in the Fluent manual, it is not physically meaningful to have a wall-adjacent height smaller than the value of the roughness height. The restriction, $z_1 > k_s$, implies a very poor resolution near the ground. Even though this limits the application of such models for the simulation of flows at pedestrian level or around low-rise buildings [3,9], it is not so restrictive in the assessment of the wind resource for large wind turbines.

In order to test the compatibility of the wall functions with the inlet profiles, a simulation on an empty domain or "virtual wind tunnel" is carried out. Here, the incoming ABL adapts to the roughness conditions given at the wall. If the domain is sufficiently long, the profiles at the outlet will be fully developed and in equilibrium with the wall conditions. Then, these profiles can be used as inlet conditions for the true geometry, whose mesh resolution near the wall should be similar to the one employed on the empty domain.

The inlet conditions (21) provided by Richards and Hoxey are used at the inlet with a roughness length of 3cm and a friction velocity of 0.57m/s (10m/s at 40m). A 3D domain with dimensions: 2000m (length), 500m (height) and 500m (width), is simulated using different roughness coefficients. A typical boundary layer development is presented in Fig. 2. The nondimensional form of Figure 2 allows an easier interpretation of the roughness length (ordinate at origin) and friction velocity (value for which the slope equals 1).

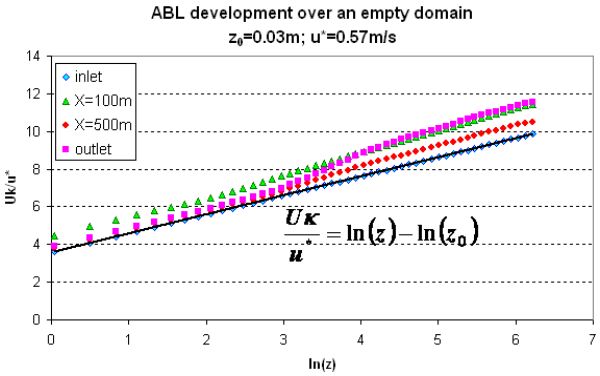

Figure 2: Development of ABL log-law over a 2km-long empty domain.

The velocity profile of the example presents the development of an internal boundary layer (IBL) with the characteristics of the wall roughness. At the outlet, the IBL has been developed up to approximately 20m following the well known $\delta_{IBL}/x \sim 1/100$ rule of thumb. The new ABL, in this example, is characterized by around 10% lower friction velocity and 20% lower roughness.

The sensibility of the inlet ABL with respect to the roughness parameters can be summarized as follows:

- As k_s increases, the roughness and friction velocity deficits decrease. For a given z_1, there is an upper limit of k_s above which the outlet ABL remains unchanged.
- As C_s increases, the outlet roughness increases and the friction velocity deficit decreases.

- The outlet roughness length depends on the height of the first cell rather than on the value of the roughness height. In general, the following expression holds for roughness lengths of the order of 3cm.

$$\frac{C_s z_1}{z_0} \approx 11.5 \tag{25}$$

Therefore, if the Alaiz site is characterized by a roughness length of 3cm and we use a mesh with z_1=0.5m, the value of C_s should be around 0.7. The value of k_s should be just bellow z_1, say k_s=0.49m. In order to minimize the friction velocity deficit, a short entry region of around 500m, between the inlet and the site, is used.

The same methodology was applied for an inlet profile characterized by high roughness (z_0=0.1m). Following the above mentioned expressions (24) or (25), the height of the first cell should be above 4m, providing a very poor resolution. At these heights the use of wall functions is not physically meaningful. The regions in Alaiz covered by high roughness are modeled using a C_s value of 1.

In general, it can be concluded that the wall functions implemented so far in Fluent 6.2 are only suitable for terrain characterized with low roughness length. A recently released 6.3 version allows the implementation of wall functions with user defined functions. This possibility will enable the definition of specific wall functions for ABL flows, which direct use the roughness length as input parameter.

5. Results

This section presents the results related to the simulations from the models specified in section 2 over Alaiz site and their assessment with field data from north wind direction. They are presented as profiles of mean velocity and turbulent intensity in the horizontal and the vertical directions. The first one corresponds to a line going from north to south across mast Alaiz3 at 40 meters above ground (line A on figure 1) whereas the second one corresponds to the vertical profiles for the three masts up to the first 100 meters.

Only the vertical profiles at the hilltop could be used for assessment as there are no measurements at the inlet of the domain. Hence, the assessment is based on the speed-up ratios between the different mast heights.

All the models reached convergence except for the Duynkerke configuration whose results are not presented.

5.1 Mean flow

In order to describe the mean flow, two non-dimensional speed-up parameters were used: fractional speed-up ratio (horizontal acceleration) and vertical speed-up (vertical acceleration).

The first one, called fractional speed–up ratio (FSR) gives an idea of how accelerated the wind speed profile is with regard to the inlet conditions.

$$FSR = \frac{V - V_{IN}}{V_{IN}} \tag{26}$$

where V is the velocity magnitude of simulated wind speed and V_{IN} the velocity magnitude at the inlet profile.

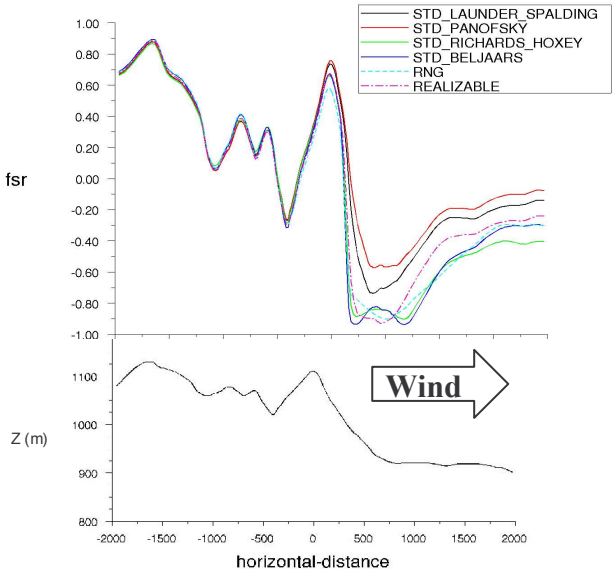

Figure 3. FSR values 40m agl. along line A. Elevation profile

Figure 3 shows the FSR evolution around Alaiz3 met mast 2 kilometres upstream and downstream and at 40 meters agl. (line A in Fig. 1). Similar trends were found upstream of mast Alaiz3 for all the tested models.

Nevertheless, discrepancies started at the hilltop and downstream. Stronger horizontal accelerations were observed for Panofsky as well as for Launder-Spalding configurations at the hilltop when comparing to the inlet profile whereas RNG showed the weakest. This trend is maintained downstream with larger differences found between the models.

The vertical speed-up profiles were normalized to the lowest level of each mast in order to assess the vertical acceleration for each turbulence model (Fig. 4). The experimental speed-up data are expressed in terms of the mean value and its standard deviation. In general good agreement was observed for the standard model with Launder-Spalding, Panofsky and Richards-Hoxey configurations. The rest of the models tend to overestimate the speed-up values at higher levels due to the correction on turbulence generation and most probably due to a too low roughness height associated to the area of the met masts.

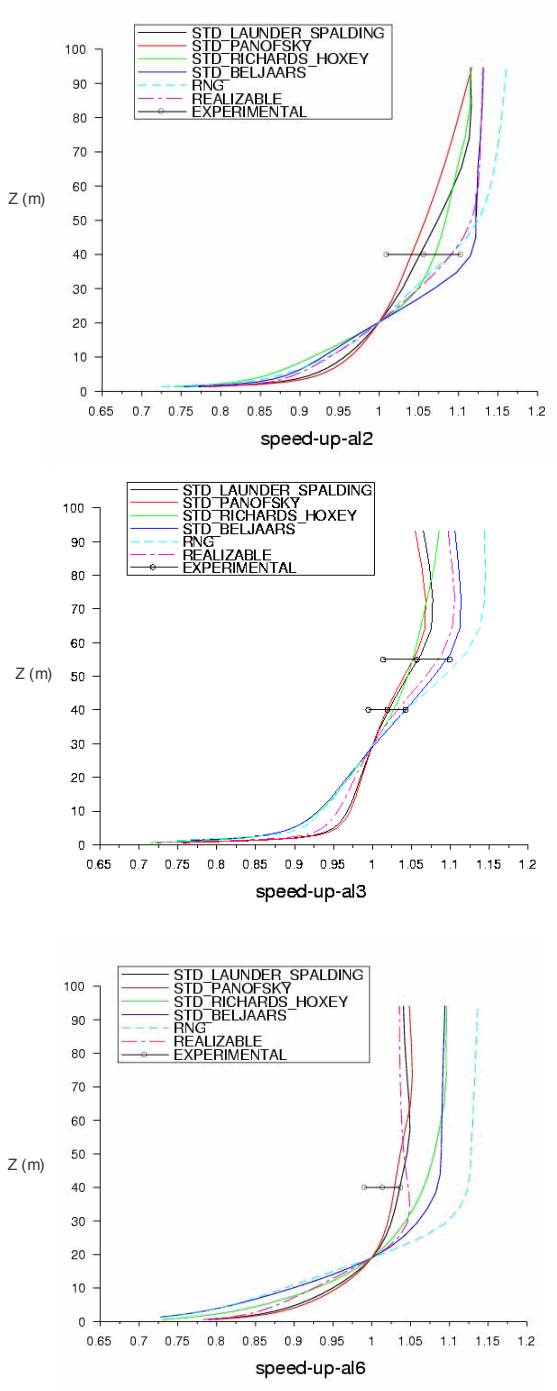

Figure 4. Vertical speed-up profiles for Alaiz2, Alaiz3 and Alaiz6

The cross-validation process consisted on simulating the values of wind speed and turbulence intensity from the lowest level of one meteorological mast to the higher levels of the other two. These simulated values are compared to the measured ones at these points.

	STD L&S	STD PNF	STD R&H	STD BLJ	RNG	RLZ
bias_V	-0.18	0.88	-0.22	1.64	1.85	0.03
mae_V	3.42	5.40	4.45	5.91	6.74	5.95

Table 1. Cross-validation. Wind speed mean absolute error (%)

The cross-validation errors in table 1 confirm the tendency. The three models specified before are in the interval 3-5.5% while the other three ones showed slightly higher errors.

5.2 Turbulent characteristics

In the same way, the turbulent flow was described through the normalized turbulent kinetic energy $k^* = k / V_{IN}^2$ along line A at 40 meters a.g.l. as well as through the vertical profiles of turbulence intensity for each met mast.

The evolution of k^* (Fig. 5) shows higher values associated to the Richards-Hoxey and Panofsky configurations in the upstream region where steep rugged profiles make the flow patterns differ considerably. Significant discrepancies were found in the downstream region characterized by different intensities according to each configuration. The Richards-Hoxey configuration corresponded to the more intense value for k^* on the lee side and the most extensive area of increased turbulence.

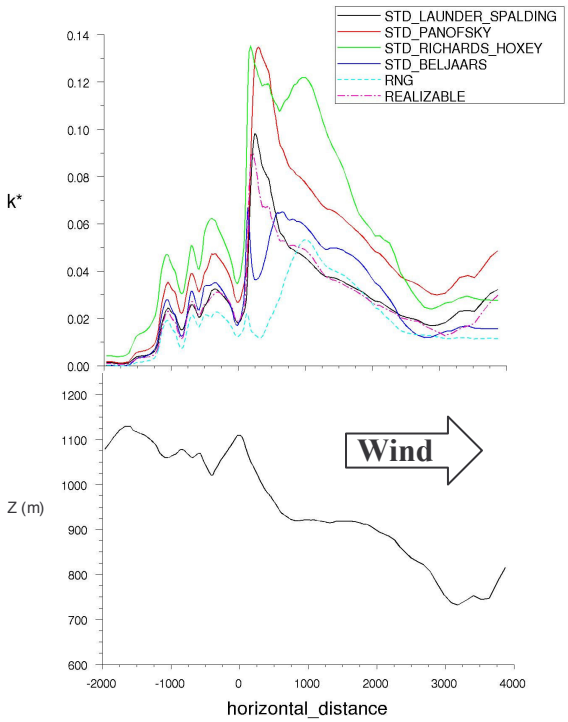

Figure 5. Normalized turbulent kinetic energy values 40 m agl. along line A. Elevation profile (m)

Important recirculation zones were observed downstream of Alaiz3 only for RNG, Realizable and Standard Richard-Hoxey models. All of them are positioned at the immediate lee side of the hilltop except for RNG, where this area was displaced further downstream than the others, mostly due to velocity gradients arising at the downstream area and making the turbulent kinetic energy to decrease rapidly in the vicinity of the hilltop.

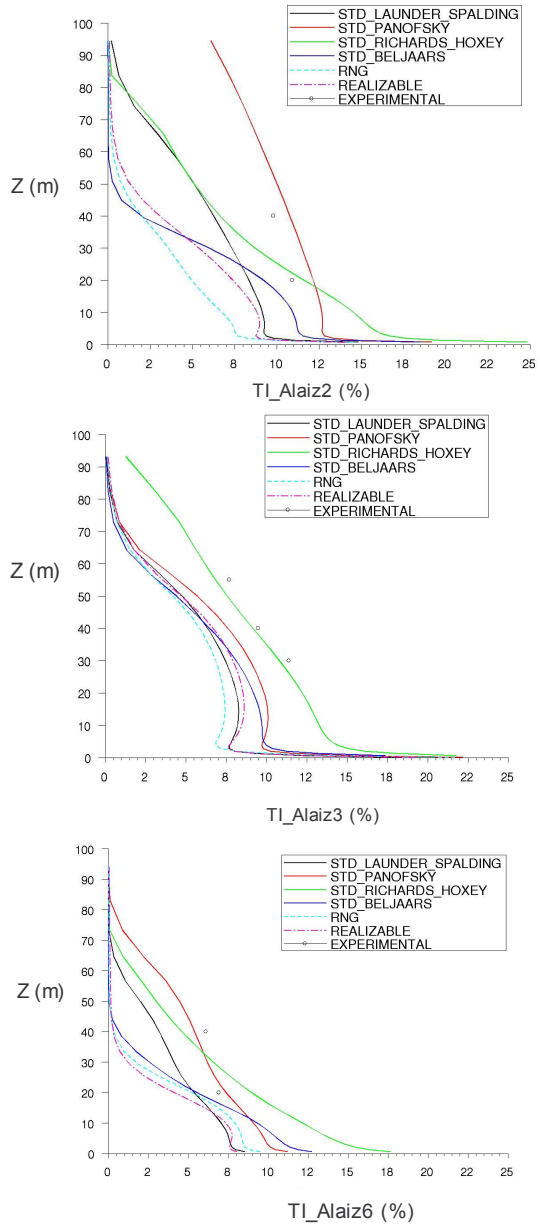

Figure 6: Vertical turbulence intensity profiles for Alaiz2, Alaiz3 and Alaiz6

The vertical profiles of turbulence intensity at the hilltop were assessed at the three meteorological masts. All the models show in general an underestimation with respect to the measurements according to the low roughness assigned to the area. Figure 6 shows that the profiles simulated by RNG and Realizable provide even less turbulent kinetic energy than the standard configurations.

The slope observed in the profiles of Launder-Spalding, Panofsky and Richard Hoxey are quite similar in Alaiz3 met mast, which is the most rugged (RIX=17%). The profiles described by the simulations carried out for the Panofsky and Richards-Hoxey combinations fits accurately the measurements, especially for Alaiz3 in the case of Richard-Hoxey and for Alaiz6 in the case of Panofsky. The rest of schemes underestimates the upper value for the less rugged masts but keeps a similar slope for the most rugged (Alaiz3).

The results are again confirmed by table 2 where the cross-validation on turbulence intensity between masts gave systematic underestimation errors mostly due to the low roughness at the site and as minimum a mean absolute error in the interval 15%-18% for Richards-Hoxey and Panofsky configurations.

	STD L&S	STD PNF	STD R&H	STD BLJ	RNG	RLZ
bias_TI	-34.63	-8.55	-3.85	-44.68	-54.67	-48.94
mae_TI	34.63	17.75	15.54	44.68	54.67	48.94

Table 2. Cross-validation. TI mean absolute error (%)

The tendency observed in the assessment of profiles for wind speed and turbulence intensity lead to a general overestimation of the first one and consequently an underestimation on the second one.

The behaviour is partly explained by the low levels of ABL roughness height k_s used in the surrounding of the masts. This height, as explained in section 4.3, is less than the theoretical value necessary to reach continuity with the wall functions and limited by the height of the first cell, low enough to get accurate results on complex terrain.

This compromise at solving turbulence in the ABL between the roughness height and the vertical resolution near the ground leads to the k-ε Standard Panofsky and Richards Hoxey schemes as the most accurate ones for the solver Fluent 6.2 from this configuration. These schemes containing minimum values of $C_{1\varepsilon}$ allow to minor the turbulence dissipation rate and to increase the turbulence kinetic energy at those roughed areas where it is underestimated.

6. Conclusions

A comparison of the simulation of ABL in complex terrain using steady-state RANS k-ε turbulence models has been carried out making use of field data from Alaiz site.

The results show that despite of the better results that the modifications on the standard k-ε model (RNG and Realizable) provide on other flow conditions, it is not necessarily the case for the simulation of the ABL on complex terrain. It seems that globally the modification of the standard model according to the Panofsky and Richards Hoxey set of constants leads to the best description of the profiles in terms of wind speed and turbulence intensity, keeping the errors within reasonable limits.

An immediate improvement would consist of optimizing the code in order to simulate accurately high roughed areas. The tasks would include adapting the resolution of the wall functions in the near wall region in order to get complete continuous flow at that area.

The results concern the simulation and assessment on the hilltop. More extensive measurements at other locations could help to extend the assessment process to other flow conditions. Of particular importance is the uncertainty on the inlet profiles, which are normally not available as in the present case. To assess its impact on

the results a sensitivity analysis should be undertaken, changing both the velocity and turbulence intensity profiles.

Further work will consist of testing anisotropic models like RSM (Reynolds Stress Models) which solve the complete Reynolds stresses and its assessment through sonic or Lidar anemometry. Comparison of turbulence intensity profiles from anisotropic (rebuilt from the normal Reynolds stresses) and isotropic models (like k-ε) could help to determine if it is worthwhile to solve the turbulence field this way at the expense of increasing computing time. Tasks like attempting to modify the set of constants at the RNG and Realizable models from the default ones could be made as long as the stability of the calculation is preserved. On the other hand, different works related to hybrid solutions from RANS-LES models are being analyzed, which will open a promising field for the next years.

Finally, a request is made for another test case, like the Askervein hill project, for complex terrain. This would significantly increase our understanding and modelling capabilities for rugged terrain sites.

7. Acknowledgements

This study has been carried out thanks to Alaiz wind farm data provided by Acciona Energía.

References

[1] Alinot, C. and Masson, C., "k-ε model for the atmospheric boundary layer under various thermal stratifications*", J. Solar Energy Engineering*, 2005, 127, 438-443

[2] Beljaars, A.C.M., Walmsley, J.L., Taylor, PA "A mixed spectral finite-difference model for neutrally stratified boundary-layer flow over roughness changes and topography". *J. Boundary-Layer Meteorology, 1987,* 38, 273–303

[3] Blocken, B., Stathopoulos, T., Carmeliet, J., "*CFD simulation of the atmospheric boundary layer – wall function problems*", J. Atmospheric Environment

[4] Brodeur, P., Sibuet-Watters, C., Masson, C., "Numerical simulations of wind distributions over very complex terrain". *44th AIAA Aerospace Sciences Meeting and Exhibit, Reno (EEUU),* 2006

[5] Cabezón, D., Iniesta, A., Ferrer E., et. al., "Comparing linear and non linear wind flow models". *Proceedings of the European Wind Energy Conference EWEC 2006*, Athens (Greece)

[6] Castro, F.A., Palma, J.M.L.M., Silva Lopes, A., "Simulation of the Askervein flow. Part I: Reynolds Averaged Navier Stokes Equations (k-ε turbulence model)", *J. Boundary Layer Meteorology*, 2003, 107, 501-530

[7] Crespo, A., Manuel, F., et. al., "Numerical analysis of wind turbine wakes", *Workshop on wind energy applications*, Delphi (Greece), 1985

[8] Fluent 6.2 User's Guide (2005), Ansys-Fluent Inc., Lebanon, 2005

[9] Franke, J., Hirsch, C., et. al., "Recommend on the use of CFD in wind engineering". *Proceedings of the International Conference on Urban Wind Engineering and Building Aerodynamics*, in: van Beeck JPAJ (Ed.), COST Action C14, Impact of Wind and Storm on City Life Built Environment, von Karman Institute, Saint-Genesius-Rode (Belgium), 2004.

[10] Kim H.G., Patel V.C., 2000, "Test of turbulence models for wind flow over terrain with separation and recirculation", *J. Boundary Layer Meteorology* 94, pp 5-21

[11] Panofsky H., Dutton J., "Atmospheric Turbulence", Wiley , New York, 1984

[12] Richards P.J., Hoxey R.P., 1993, "Appropiate boundary conditions for computational wind engineering models using the K-EPS turbulence model", *J. Wind Engineering and Industrial Aerodynamics*, pp. 46-47

[13] Taylor, P.A., Teunissen, H.W., "*The Askervein Hill project: overview and background data*". J. Boundary-Layer Meteorology, 1987, 39, 15–39

[14] Troen, I., Lundtang, E., "European Wind Atlas", Riso National Laboratory, Denmark, 1989

[15] Undheim O., Anderson H.I., Berge E., "Non-linear, microscale modelling of the flow over Askervein hill*", J. Boundary Layer Meteorology*, 2006, 120, 5-21

[16] Undheim O., "Comparison of turbulence models for wind evaluation in complex terrain*", Proceedings of the European Wind Energy Conference EWEC 2003*, Madrid (Spain)